Magn Reson Mater Phy (2007) 20:19–25
DOI 10.1007/s10334-006-0065-8

RESEARCH ARTICLE

Parallel acquisition for effective density weighted imaging: PLANED imaging

Oliver M. Geier · Dietbert Hahn · Herbert Köstler

Received: 29 May 2006 / Accepted: 6 December 2006 / Published online: 20 January 2007

Abstract
Objective Density weighted phase-encoding has proven to be a highly efficient method for *k*-space sampling as it improves the localization properties and increases the signal-to-noise ratio for extended samples at the same time. But either density weighted imaging lengthens the minimum scan time or, if the Nyquist criterion is violated in parts of the sampled *k*-space, undersampling artefacts occur. Purpose of this work was to combine density weighted imaging and parallel imaging techniques to improve the spatial response function and consequently the signal-to-noise ratio without spoiling image quality by undersampling artefacts.
Materials and Methods Images were acquired with parallel acquisition for effective density weighted imaging (PLANED imaging) and compared to results sampled with conventional Cartesian phase-encoding with the same spatial resolution and the same number of excitations.
Results Both in vivo and phantom measurements recorded with the PLANED method revealed a considerable enhancement of the signal-to-noise ratio and a remarkable reduction of Gibbs artefacts compared to standard Cartesian imaging.
Conclusion It has been demonstrated that PLANED improves image quality by suppressing truncation artefacts and increasing the SNR without lengthening the measurement time.

Keywords Density weighted imaging · Parallel imaging · Non-Cartesian imaging · Truncation artefacts · Signal-to-noise ratio

O. M. Geier (✉) · D. Hahn · H. Köstler
Institut für Röntgendiagnostik,
Universität Würzburg, Josef-Schneider-Str.2,
97080 Würzburg, Germany
e-mail: oliver.geier@rikshospitalet.no

O. M. Geier
Department of Medical Physics,
Rikshospitalet-Radiumhospitalet University Hospital,
Sognsvannsveien 20, Oslo, Norway

Introduction

The finite sampling in *k*-space leads to severe contamination between different pixels in standard Cartesian MRI. This signal contamination from neighbouring regions can be described by the shape of the spatial response function (SRF). The SRF reflects the spatial origin of signals contributing to a distinct pixel [1]. Often the effect of a finite sampling in *k*-space can be observed as the so-called "Gibbs ringing" artefact. A common method to improve the shape of the SRF is to employ *k*-space filters, i.e., to attenuate phase encoding steps in the outer parts of sampled *k*-space. This reduces the side lobes of the SRF and consequently the contamination from neighbouring regions. While the broadening of the main lobe of the SRF can be compensated by choosing a larger k_{max}, the application of retrospective *k*-space filters always results in a loss of signal-to-noise ratio. To avoid this drawback the *k*-space filtering may be applied during data acquisition [2–7], i.e., the data are sampled in an acquisition or density weighted manner. In acquisition weighted imaging *k*-space points in the centre of *k*-space are sampled more often then those in the outer parts. A continuous distribution of the sampling density may be achieved by varying the distance between adjacent *k*-space points as proposed by Greiser et al. [2,3]. The key idea of acquisition or density

weighted imaging is to apply no density correction in the reconstruction in contrast to other non-Cartesian imaging techniques which perform density correction explicitly [8–10] or implicitly [11,12]. Acquisition and density weighted imaging have been successfully applied to spectroscopic imaging [2,4,5] and non-proton imaging [3]. In these studies not only improved localization properties of acquisition and density weighted imaging were found but also the SNR for extended objects could be increased by the suppression of the negative contamination from neighbouring regions. The extent of this effect depends on the morphological geometry [5]. For typical clinical proton imaging these methods have not become accepted as they either lengthen the minimum scan time [13], or if the Nyquist criterion in the outer parts of *k*-space is violated, suffer from undersampling artefacts [2]. The aim of this work is to present a new technique that combines efficiently density weighted sampling for optimal SNR and minimal contamination from neighbouring regions with parallel imaging to eliminate undersampling artefacts and limit the scan time.

Principle of PLANED imaging

PLANED imaging combines density weighted imaging with parallel imaging techniques. In contrast to conventional Cartesian imaging (see Fig. 1a) in PLANED imaging, the *k*-space sampling is performed in a density weighted manner (see Fig. 1b). In order to achieve the same resolution as for an image acquired with a Cartesian sampling, i.e., the SRF at 64% of maximum intensity has the same width, $k_{y,\max}$ has to be chosen larger in PLANED imaging [2]. The basic idea of PLANED imaging is to fill the gaps of the undersampled parts of *k*-space by parallel imaging techniques, such as GRAPPA [14] or SENSE [11] to avoid undersampling artefacts while maintaining the distribution of the sampling density defined by the weighting function.

If an oversampled part of *k*-space exists, it can be used for inherent self-calibration for the parallel imaging reconstruction [15,16] and no additional data have to be recorded.

Methods

Acquisition protocol

Written informed consent was obtained before each study. All measurements were performed on a 1.5 T scanner (Magnetom Symphony, Siemens) using a 12-channel array coil (6-channel body coil anterior and 6-channel posterior) and 8 receiver channels. Both phantom and in vivo measurements were carried out in transversal slice orientation and the array coils were positioned above and below the object.

Images generated with the PLANED method were compared to conventional Cartesian sampled images with the same spatial resolution and identical parameters, including number of phase encoding steps except for different phase encoding gradients k_y. Images were recorded with a standard spin echo sequence (TE = 15 ms, TR = 525 ms). The raw data matrix was set to 256×512 for the phantom measurement and to 256×256 for the in vivo measurement. The density distribution of the phase encoding direction is presented in Fig. 2. The sampling density followed a cosine square function [Hanning function, $H(k)$] but was set to 1/3 in the outer part to avoid excessive noise enhancement in the parallel imaging reconstruction:

$$w(k) = H(k) \quad or\ 1/3 \quad \text{whichever is larger} \tag{1}$$

For 256 phase encoding steps $w(k)$ has to be set to 1/3 for k_y for the range indicated in Fig. 2.

PLANED and Cartesian imaging achieve the same spatial resolution, if the widths at 64% of the maximum intensity of their SRFs are equal [4]. Therefore the phase encoding steps of the PLANED experiments

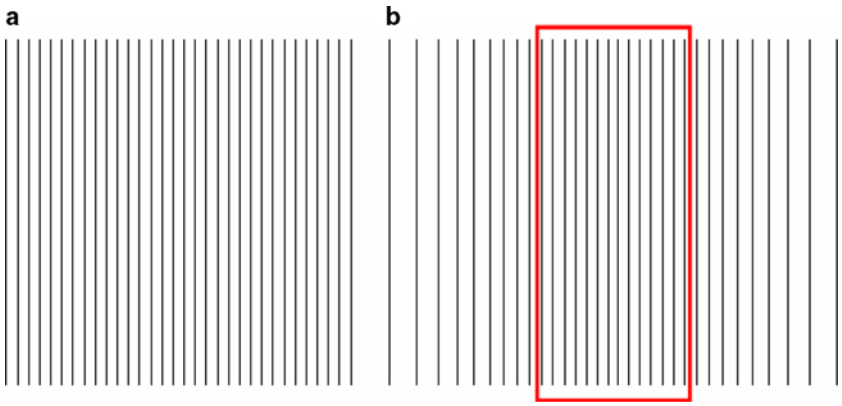

Fig. 1 Schematic representation of the sampling for non-weighted Cartesian imaging (*left*) and for PLANED imaging (*right*). The *red rectangle* shows the part of the *k*-space where the Nyquist criterion is fulfilled

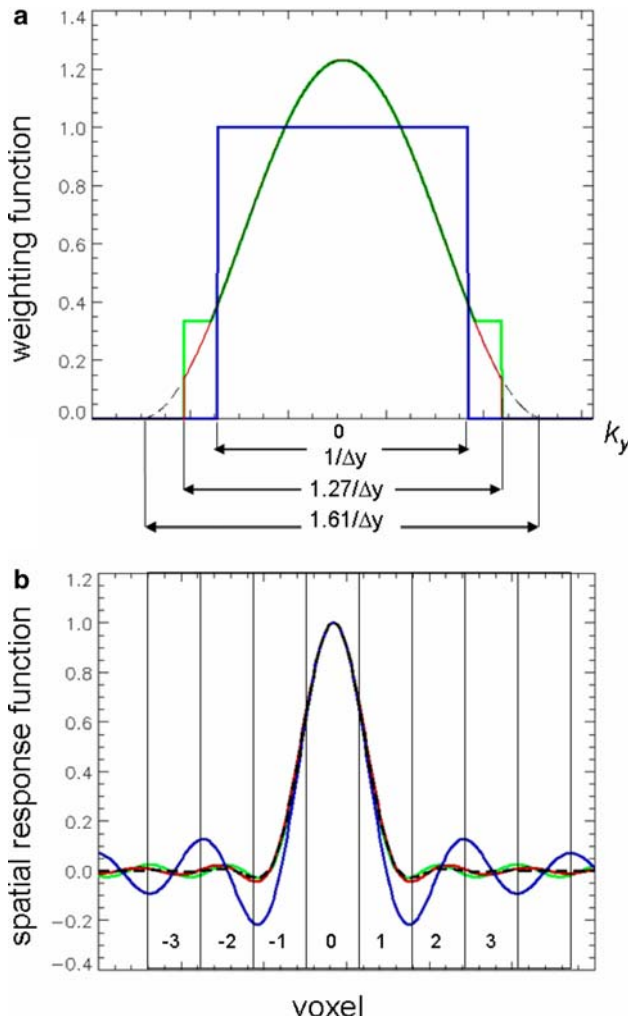

Fig. 2 *k*-space weighting functions (*top*) and the corresponding SRFs (*bottom*) for the sampling of the PLANED experiment (*green*) and the final filtering (*red*) compared to a Cartesian experiment (*blue*). The calculated SRFs (*bottom*) indicate that both experiments have the same spatial resolution. For comparison the original cosine square-function (*black*) and the corresponding spatial response function (*dashed line*) are also displayed

were adjusted as described by Pohmann and von Kienlin [4], i.e., the value for $w_{\max}$ and $k_{y,\max}$ were chosen larger for the PLANED sampling scheme. These parameters have been calculated to $k_{y,\max} = 1.61$ and $w_{\max} = 1.23$ for acquisition weighting in one dimension. This assures that the integral over $w(k)$ yields exactly the same total number of accumulations NA and the same spatial resolution as for the corresponding unweighted Cartesian experiment. Figure 2b displays the SRF for Cartesian, acquisition weighted and PLANED imaging, as it was used in the presented experiments and shows that the different used sampling schemes lead to the same resolution.

To calculate the signal-to-noise ratio two images with identical parameters were recorded for conventional Cartesian imaging and PLANED imaging, respectively. The signal-to-noise ratio within a region of interest was calculated by the ratio of the average and the standard deviation of the difference of both images.

The point spread function in phase encoding direction was determined as the derivative of the edge spread function. The latter was taken from a row perpendicular to the edge of the phantom as shown in Fig. 5.

Image reconstruction

Image reconstruction was carried out using custom-built software written in Interactive Data Language (Research Systems Inc., Boulder, CO, USA). To consider the coil profiles in x direction the reconstruction process was carried out in the k_y-x space, i.e., before the PLANED reconstruction the signal was Fourier transformed in the direction of the frequency encoding. The reconstruction was performed independently for each position in x-direction. In the oversampled part data were gridded onto a dense Cartesian grid for every coil element using a Kaiser–Bessel function as it is proposed in [9]. To reconstruct points for every coil element on a Cartesian grid in the undersampled part a PARS [15] like GRAPPA [14] algorithm was applied. To calculate the signal for an aiming point on the Cartesian grid the four closest measured neighbour points were selected and the corresponding distances were determined. Using these distances the GRAPPA factors were determined in the oversampled part of k-space as described in detail below. This allowed the calculation of k-space points on a Cartesian grid fulfilling the Nyquist criterion also in the outer part.

The complete Cartesian k-space, i.e., the gridded inner part and the GRAPPA-reconstructed outer part, was multiplied by a cosine square filter to restore basically the sampled density distribution. The filtered k_y-spaces for every coil element were subsequently Fourier transformed and the final image was obtained by taking the square root of the sum of squares of the single coil images.

Determination of GRAPPA-factors

For every point on a Cartesian grid k_y in the outer part of the k-space, GRAPPA reconstruction factors were determined independently. To calculate the signal for every aiming point on the Cartesian grid the $N_b = 4$ closest measured neighbour points $(k_{y,n1}, k_{y,n2}, k_{y,n3}, k_{y,n4})$ were selected and the corresponding distances were determined ($\Delta k_{y,n1} = k_{y,n1} - k_y$). In the oversampled part the measured data were sinc-interpolated in k_y direction. The measured points in the oversampled part of the k-space were used as auto calibration signals for

four interpolated points at the calculated distances. The signal for the coil j at a point k_y is given by

$$S_j^{\mathrm{ACS}}(k_y) = \sum_{l=1}^{L} \sum_{b=0}^{N_b-1} n(j,b,l) S_l\left(k_y + \Delta k_{y,nb}\right), \qquad (2)$$

where l is the index of all coils and b denotes the individual neighbour point $(0 - N_b - 1)$. By setting up a system of equations for all measured point in the oversampled part of the k-space the different complex coil weights $n(j,b,l)$ were calculated by a singular value decomposition. Using these coil weights the signals at Cartesian positions in the undersampled k-space were calculated.

Comparison of PLANED to standard density weighted imaging

To compare the PLANED method with standard density weighting and to investigate the influence of the aliasing artefacts due to the violation of the Nyquist criterion, the density weighted raw data were also reconstructed without parallel image reconstruction, i.e., using a regridding algorithm for the whole k-space. For this density weighted reconstruction the k-space was weighted by the same function as for the PLANED reconstruction.

Results

Figure 3 shows the results of measurements of a test object recorded with the Cartesian, the PLANED and the density weighted technique. For the PLANED and the density weighted image the same raw data were used, but different reconstruction algorithms were applied. The Cartesian image has the lowest SNR and clearly reveals truncation artefacts in phase encoding direction, which can be observed as a line pattern at the edge of the phantom. The PLANED and the density weighted image show no Gibbs ringing in phase encoding direction. Both images exhibit the same SNR, but the density weighted image suffers from undersampling artefacts. These are visible as line patterns in the image at a distance at least 1/3 of the FOV from the signal producing structure. This corresponds to a maximum undersampling of a factor of three. The best image quality is achieved by the PLANED imaging technique. The improved SRF results not only in the elimination of truncation and undersampling artefacts but also in the increase of SNR, in this example by 34% compared to the Cartesian sampled image.

To test whether the spatial resolution Δy is identical for both images, the magnitude of the spatial response function was calculated from the edge spread function in the row indicated by a red line in Fig. 5 for the Cartesian and the PLANED imaging technique. The magnitudes of the SRFs are presented in Fig. 4. The results confirm experimentally that within the range of measurement errors both images have the same spatial resolution. Additionally the strong suppression of truncation artefacts for PLANED can be observed in the SRF, too. In contrast to the SRF obtained from the Cartesian image the SRF of the PLANED image shows much less pronounced side lobes.

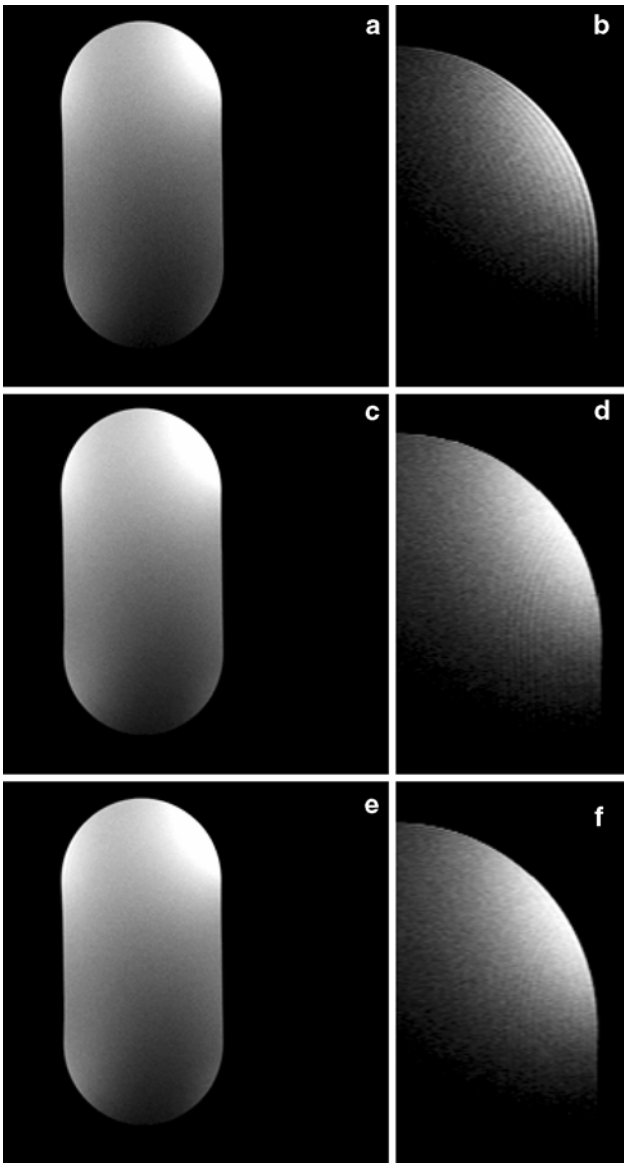

Fig. 3 Comparison of images recorded with standard Cartesian sampling (**a**, **b**), standard density weighted imaging (**c**, **d**) and the PLANED technique (**e**, **f**). The *right column* shows the same images zoomed to a quarter of the original image size. Images **a**, **c**, **e** and **b**, **d**, **f** are windowed equally, respectively

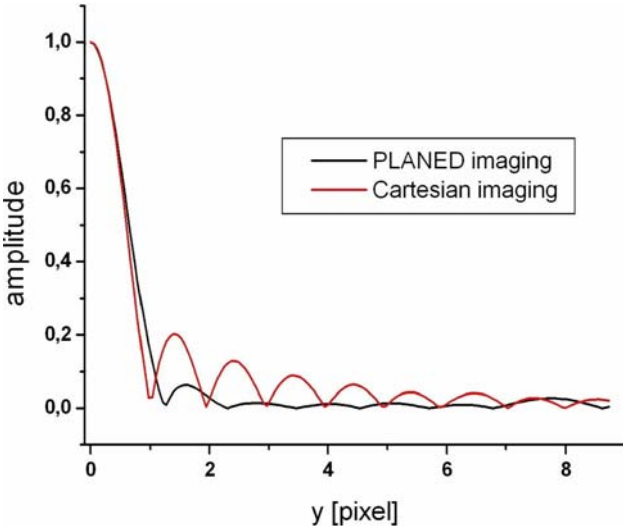

Fig. 4 Comparison of the measured spatial response functions resulting from the Cartesian image shown in Fig. 3a and the PLANED image in Fig. 3e

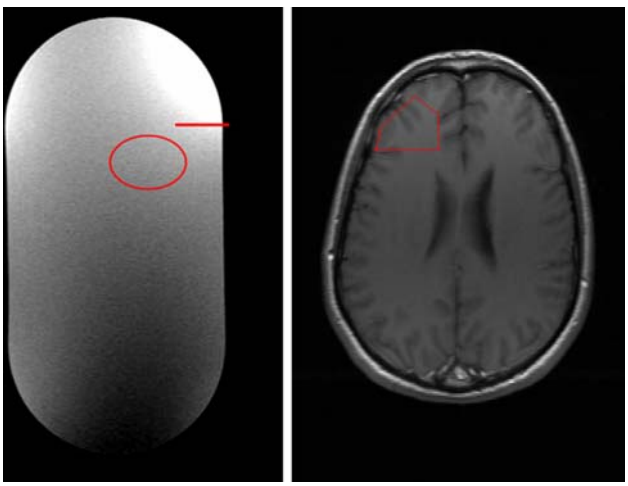

Fig. 5 Position of the line where the SRFs shown in Fig. 4 were determined and position of the ROIs for the determination of the SNR

An in vivo measurement of a human brain is presented in Fig. 6. The Cartesian image again reveals Gibbs ringing in the phase encoding direction. This is not observable in the density weighted image and in the PLANED image. While the density weighted image is corrupted by undersampling artefacts, these are not observable in the image, recorded with the PLANED technique.

The SNR measurements yield an enhancement of 17% for the images obtained by the PLANED method.

The ROIs which were used for the calculation of the SNR are indicated in Fig. 5.

Discussion

In this work a new technique, parallel acquisition for effective density weighted imaging, is proposed and tested on phantoms and on in vivo applications. The proposed technique suppresses truncation artefacts and enhances considerably the signal-to-noise ratio of MR images of extended samples compared to conventional methods.

Acquisition and density weighted imaging methods have proven their capability to reduce the cross-talk between different pixels. At the same time these methods improve the SNR to an extent depending on the morphological geometry. The SNR gain originates from the suppression of the negative side lobes in the SRF compared to Cartesian imaging. Up to now the use of acquisition and density weighted imaging in clinical routine imaging was hampered by the increased minimum scan time or, if the Nyquist criterion is violated, by aliasing artefacts.

One of the most important technical advances in the last decade was the introduction of parallel imaging techniques. Parallel imaging reconstruction allows one to remove aliasing from undersampled data sets at the prize of a SNR amplification of a factor of g [14].

In this study the first results of a combination of density weighted and parallel imaging are presented. In the proposed implementation of PLANED imaging the sampling density was chosen according to a slightly modified cosine-square function. A cosine-square function is a common k-space filter function that offers a favourable spatial response function [17]. The sampling density in our experiments was restricted to values larger 1/3 to keep the noise amplification factor (g-factor) by parallel image reconstruction low, even for our not optimized hardware. It could be shown that the effect of small deviations from the cosine-square filter function on image SNR and SRF is minimal. The filling of the gaps in the sparse k-space was performed by a GRAPPA [14], or PARS [15] algorithm. But of course, PLANED imaging is not restricted to the use of the modified cosine-square filter or a GRAPPA reconstruction. Other filter functions like Kaiser–Bessel functions or numerically optimized functions [8] for a desired SRF may also be used. This also includes particular applications like edge enhancement filters for certain applications. Likewise the parallel imaging method included in our reconstruction can be substituted by any other parallel imaging technique and calibration method. In the implemented GRAPPA-reconstruction only four neighbouring points contributed to the reconstructed k-space points. According to the findings in [14] the usage of four neighbouring points results in the same reconstruction quality

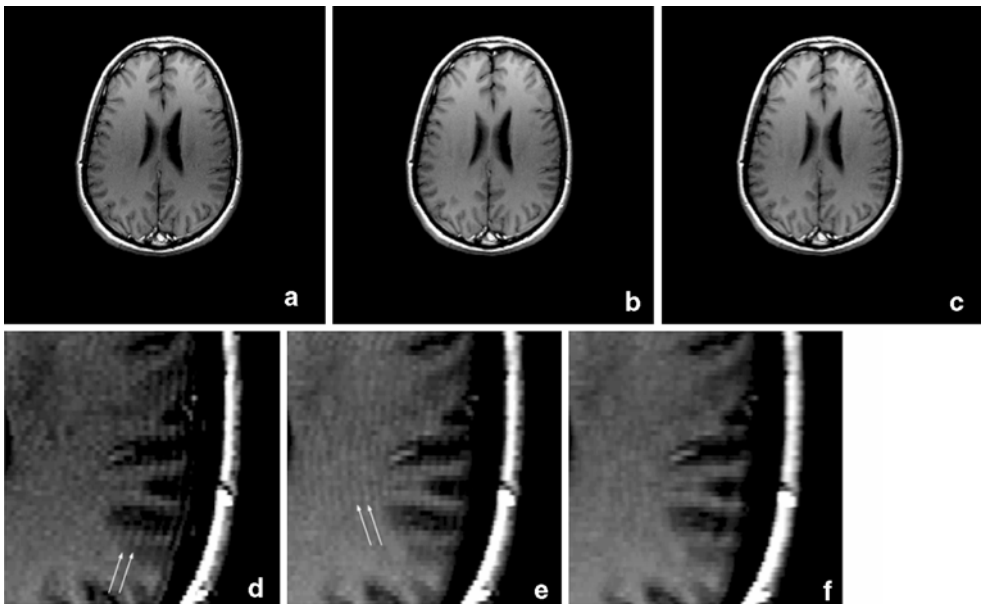

Fig. 6 In vivo images of the human brain recorded with standard Cartesian sampling (*left*), standard density weighted imaging (*middle*) and with the PLANED technique (*right*). The stripes visible in Fig. 6e can be attributed to undersampling artefacts, whereas in 6d Gibbs ringing is visible

as a reconstruction with more points. But PLANED reconstruction is not limited to this particular choice. PLANED imaging may certainly profit from modified GRAPPA algorithms where regularization is performed after the singular-value decomposition for large coil arrays [18,19]. But also other parallel techniques working either in the *k*-space [20–23], image space [10,11] or hybrid techniques [12] can be used in the reconstruction of PLANED imaging. In this study coil sensitivity information was extracted from the densely sampled centre of the *k*-space. This self calibration can be applied to all cases were at least a part of *k*-space fulfils the Nyquist criterion. But coil profile information may also be determined in a separate prescan [11] or by completely filling a dense *k*-space in dynamic imaging [24–28].

In the examples presented in this study the spatial resolution and the number of phase encoding steps were kept constant to compare Cartesian and PLANED imaging. But it is also possible to design a PLANED sequence that shows the same spatial resolution and the same SNR as the Cartesian technique. The presented results would correspond to a reduction of the acquisition time by a factor of about 1.4–1.8.

PLANED imaging is not restricted to a certain type of pulse sequence, as spin echo imaging. First results using gradient echo PLANED imaging (not shown in this work) indicate that the PLANED principle can be applied to all phase encoded pulse sequence.

The highest impact of PLANED imaging is expected in applications which are limited by the signal-to-noise ratio. Among these are fMRI studies, where the low SNR results in long acquisition times. But clinical images that SNR limited because they are recorded during breath hold or in real time should profit from the SNR gain in PLANED imaging. A special importance is expected for the application of the PLANED technique for 3D imaging. As in 3D imaging typically two dimensions are phase encoded the SNR gain in PLANED imaging should be squared compared to 2D MR imaging. PLANED imaging may substitute averaging and the need for higher field strength in some applications but it may also be combined with these techniques to allow new applications of MR imaging.

Conclusion

The new proposed technique, PLANED imaging, was applied to phantom and in vivo studies. The results showed that PLANED improves the image quality by suppressing truncation artefacts and increasing considerably the signal-to-noise ratio. Thus PLANED opens the way for higher SNR and shorter scan times in most MR imaging applications.

References

1. Kienlin M, Pohmann R (1998) Spatial resolution in spectroscopic imaging. In: Blümler P, Blümich B, Botto R, Fukushima E (eds.) Spatially resolved magnetic resonance. Wiley-VCH, Weinheim, pp 3–20

2. Greiser A, von Kienlin M (2003) Efficient *k*-Space sampling by density-weighted phase-encoding. Magn Reson Med 50:1266–1275
3. Greiser A, Haase A, von Kienlin M (2005) Improved cardiac sodium MR imaging by density weighted phase-encoding. J Magn Reson Imag 21:78–81
4. Pohmann R, von Kienlin M (2001) Accurate phosphorous metabolite images of the human heart by 3D acquisition-weighted CSI. Magn Reson Med 45:817–826
5. Köstler H, Beer M, Landschütz W, Buchner S, Sandstede J, Pabst T, Kenn W, Neubauer S, von Kienlin M, Hahn D (2001) ^{31}P-MR-Spektroskopie aller Wandabschnitte des menschlichen Herzens bei 1,5 T mit akquisitionsgewichteter Chemical-shift-Bildgebung. Fortschr Röntgenstr 173:1093–1098
6. Mareci TH, Brooker HR (1984) High resolution magnetic resonance spectra from a sensitive region defined with pulsed field gradients. J Magn Reson 57:157–163
7. Ponder SL, Twieg DB (1994) A novel sampling method for ^{31}P spectroscopic imaging with improved sensitivity, resolution and side lobe suppression. J Magn Reson B 104:85–88
8. Jackson JI, Meyer CH, Nishimura DG (1991) Selection of a Convolution Function for Fourier Inversion Using Gridding. IEEE Trans Med Imaging 10:473–478
9. Pipe GP, Menon P (1999) Sampling density compensation in MRI: rationale and an iterative numerical solution. Magn Reson Med 41:179–186
10. Pruessmann KP, Weiger M, Bornert P, Boesiger P (2001) Advances in sensitivity encoding with arbitrary *k*-space trajectories. Magn Reson Med 46:638–651
11. Pruessmann KP, Weiger M, Scheidegger MB, Boesiger P (1999) SENSE: sensitivity encoding for fast MRI. Magn Reson Med 42:952–962
12. Kyriakos WE, Panych LP, Kacher DF, Westin CF, Bao SM, Mulkern V, Jolesz FA (2000) Sensitivity profiles from an array of coils for encoding and reconstruction in parallel (SPACE RIP). Magn Reson Med 44:301–308
13. Parker DL, Gullberg GT, Frederick PR (1987) Gibbs artifact removal in magnetic resonance imaging. Med Phys 14:640–645
14. Griswold MA, Jakob PM, Heidemann RM, Nittka M, Jellus V, Wang J, Kiefer B, Haase A (2002) Generalized autocalibrating partially parallel acquisitions (GRAPPA). Magn Reson Med 47:1202–1210
15. Yeh EN, McKenzie CA, Ohliger MA, Sodickson DK (2005) Parallel magnetic resonance imaging with adaptive radius in *k*-space (PARS): constrained image reconstruction using *k*-space locality in radiofrequency coil encoded data. Magn Reson Med 53:1383–1392
16. Yeh EN, Stuber M, McKenzie CA, Botnar RM, Leiner T, Ohliger MA, Grant AK, Willig-Onwuachi JD, Sodickson DK (2005) Inherently self-calibrating non-Cartesian parallel imaging. Magn Reson Med 54:1–8
17. Mareci TH, Brooker HR (1991) Essential considerations for spectral localization using indirect gradient encoding of spatial information. J Magn Reson 92:229–246
18. Lin FH, Kwong KK, Belliveau JW, Wald LL (2004) Parallel imaging reconstruction using automatic regularization. Magn Reson Med 53:559–567
19. Sodickson DK (2000) Tailored SMASH image reconstructions for robust in vivo parallel MR imaging. Magn Reson Med 44:243–251
20. Jakob PM, Griswold MA, Edelman RR, Sodickson DK (1998) AUTO-SMASH: a self-calibrating technique for SMASH imaging. Simultaneous acquisition of spatial harmonics. Magma Magn Reson Mater Phys 7:42–54
21. Heidemann R, Griswold M, Haase A, Jakob PM (2001) VD-Auto-SMASH imaging. Magn Reson Med 45:1066–1074
22. Griswold MA, Blaimer M, Breuer F, Heidemann RM, Mueller M, Jakob PM (2005) Parallel magnetic resoance imaging using the GRAPPA operator formalism. Magn Reson Med 54:1553–1556
23. Heidemann R, Griswold MA, Jacob PM (2003) Fast parallel image reconstructions with non-Cartesian trajectories. Proc Int Soc Mag, Reson Med 11:2347
24. Koestler H, Landschütz W, Sandstede J, Lipke C, Hahn D (2000) Abstract: heart perfusion imaging using SENSE Radiology 217 (P) supplement, 464
25. Kellman P, Epstein FH, Mc Veigh ER (2001) Adaptive sensitivity encoding incorporating temporal filtering (TSENSE). Magn Reson Med 45:846–852
26. Köstler H, Sandstede JJW, Lipke C, Landschütz W, Beer M Hahn D (2003) Auto-SENSE perfusion imaging of the whole human heart. J Magn Reson Imaging 18:702–708
27. Köstler H, Beer M, Ritter C, Hahn D, Sandstede J (2004) Auto-sense view-sharing cine cardiac imaging. MAGMA Magn Reson Mater Phys 17:63–67
28. Breuer FA, Kellmann P, Griswold PA, Jakob PM (2005) Dynamic autocalibrated parallel imaging using temporal GRAPPA (TGRAPPA). Magn Reson Med 53:981–985